Talanta 108 (2013) 165–170

Contents lists available at SciVerse ScienceDirect

Talanta

journal homepage: www.elsevier.com/locate/talanta

Disposable immunosensors for C-reactive protein based on carbon nanotubes field effect transistors

Celine I.L. Justino [a,*], Ana C. Freitas [a,b], José P. Amaral [c], Teresa A.P. Rocha-Santos [a,b], Susana Cardoso [c], Armando C. Duarte [a]

[a] Department of Chemistry & CESAM, University of Aveiro, Campus de Santiago, 3810-193 Aveiro, Portugal
[b] ISEIT/Viseu, Instituto Piaget, Estrada do Alto do Gaio, Galifonge, 3515-776 Lordosa, Viseu, Portugal
[c] INESC-MN, Rua Alves Redol 9, 1000-029 Lisbon, Portugal

ARTICLE INFO

Article history:
Received 12 November 2012
Received in revised form
25 February 2013
Accepted 2 March 2013
Available online 13 March 2013

Keywords:
Carbon nanotubes
Cardiovascular diseases
C-reactive protein
Disposable biosensors
Field effect transistor

ABSTRACT

Label-free immunosensors based on single-walled carbon nanotubes field effect transistor (NTFET) devices were developed for the detection of C-reactive protein (CRP) which is currently the best validated inflammatory biomarker associated with cardiovascular diseases. The immunoreaction principle consists in the direct adsorption of CRP specific antibodies (anti-CRP) to single-walled carbon nanotubes (SWCNTs) networks. Such anti-CRP are the molecular receptors of CRP antigens which, in turn, can be detected by the developed NTFET devices in a linear dynamic range of 10^{-4}–10^{2} μg/mL. Thus, typical values of CRP (in blood serum) for healthy persons (<1 μg/mL), and higher levels (>5 μg/mL) corresponding to pathological states, can be both detected with the NTFET immunosensors, becoming an advantageous alternative as the basis for the development of analytical instrumentation for assessment of risk of occurrence of cardiovascular diseases. A log–log linear regression was applied to the experimental data with a correlation coefficient of $r=0.9962$ ($p<0.001$), and there is no statistical difference (from ANOVA) between individual NTFET devices ($p=0.9582$), demonstrating acceptable reproducibility. According to the experimental results, the estimate of detection limit (LOD, 10^{-4} μg/mL) is 3-fold lower than that of some conventional immunoassay techniques for blood serum (e.g., LOD of 0.2 μg/mL for high-sensitivity enzyme-linked immunosorbent assay), and the dynamic range (10^{-4}–10^{2} μg/mL) is about 6-fold higher. Furthermore, this simple and low-cost methodology allows the use of sample volumes as low as 1 μL for the label-free detection of CRP.

1. Introduction

C-reactive protein (CRP) is produced in serum by hepatocytes and regulated by inflammatory cytokines, mainly by interleukin-6; it has been considered as the best current validated inflammatory biomarker [1] and functions as an acute phase protein in response to tissue damage, infection, and systemic inflammation.

The monitoring of CRP levels is important to predict the risk of atherosclerotic diseases, including cardiovascular disease, which is the main cause of death worldwide [2]. The risk of cardiovascular diseases has been considered low if the levels of CRP in serum are below 1.0 μg/mL and, in turn, it becomes elevated when levels of CRP are higher than 3.0 μg/mL [1]. When levels of CRP are as high as 3.0 μg/mL, it functions as a significant indicator for the chronic cardiovascular diseases including acute coronary syndromes. High levels between 10 and 50 μg/mL can also be found in late pregnant women and viral infections, and even higher levels, between 50 and 200 μg/mL, are related to bacterial infections and active inflammation [3]. Then, biosensing systems as well as other analytical techniques should cover the whole concentration range of interest, i.e., they may be capable to evaluate levels of CRP lower than 1.0 μg/mL and higher than 50 μg/mL.

Clinical immunochemical methods based on high sensitivity assays, i.e., immunoturbidimetric, immunochemiluminometric, and immunonephelometric assays, as well as enzyme linked immunosorbent assays have been traditionally used to the detection of CRP in blood serum with limits of detection (LOD) ranging from 0.03 to 0.2 μg/mL and detection range between 5 and 10 μg/mL of CRP [4,5]. By definition, immunoassays are biochemical tests for quantifying a substance based on its ability to bind to an antibody (immunoreaction); they require expensive instrumentation, sample pre-treatment protocols, laborious work, and rigid operational procedures, as well as they are time consuming, and the detection is indirect, since they are based on optical transduction and one of the reagents is labeled.

Besides immunoassays, the immunosensors based on electrochemical/optical platforms (physical transducers) such as surface plasmon resonance, field effect transistors, and quartz crystal microbalance are label-free, ease of use, less expensive, with

* Corresponding author. Tel.: +351 232910100; fax: +351 232910183.
E-mail address: celinejustino@ua.pt (C.I.L. Justino).

0039-9140/$ - see front matter © 2013 Elsevier B.V. All rights reserved.
http://dx.doi.org/10.1016/j.talanta.2013.03.007

minimal requirements of sample preparation, and the output signal is obtained directly from sensor software [6]. In electrochemical immunosensors, the reaction between antigen and antibody is detected and converted, through a transducer, to an electrical signal, which is processed and displayed as output signal. Meyer et al. [7] developed a magnetic immunosensor with acceptable values for LOD (25.0 ng/mL) on a large dynamic linear range (0.025–2.5 μg/mL). However, Meyer et al. [7] highlighted some disadvantages in the magnetic immunosensor such as the high sample size (0.5 mL) and large time required for measurement (30 min). Bini et al. [8] proposed an optical RNA-based aptasensor based on the surface plasmon resonance method, with a lower LOD (5×10^{-3} μg/mL) than that obtained by Meyer et al. [7]; however, the method is labor intensive and requires expensive equipment for measurement of CRP. In turn, Yang et al. [9] and Quershi et al. [10] proposed biosensing systems based on magnetic principles, a microfluidic system and a capacitive immunosensor, with LOD of 1.25×10^{-2} and 2.5×10^{-2} μg/mL, respectively. Therefore, disposable, rapid, simple, and low-cost biosensing instrumentation for CRP has not yet been reported.

Nanoelectronic devices have been thought to increase the analytical performance of biosensing systems, since they can incorporate various types of nanomaterials, such as single-walled carbon nanotubes (SWCNTs). SWCNTs display particular electrical and transport properties, and high electron transfer reactions due to the presence of all carbon atoms in their surface; SWCNTs also have a large surface area with the possibility of functionalization with different molecules for the specific detection of various analytes, such as proteins, DNA, and even viruses [11]. When integrated as conducting channel in a field effect transistor (NTFET), changes in electrical current are observed since adsorption of biomolecules to receptor analytes (e.g., antibodies) can occur [12–15]. Networks of SWCNTs have been successfully applied to the development of useful NTFET biosensors for the detection of DNA [16], human immunoglobulin G [17,18], and Aspergillus flavus fungi [19], among others. The networks of SWCNTs allow a much larger surface area than individual nanotubes, and the sensing devices fabricated from such networks average the properties of a large number of random individual SWCNTs [20]. On the other hand, the use of such miniaturized devices allows the use of small volumes of sample, and the enhancement of analytical performance, for example, in terms of sensitivity and LOD. A few biosensing systems have used nanomaterials for the detection of CRP; for example, Buch and Rishpon [21] developed an electrochemical immunosensor based on multi-walled carbon nanotubes-modified screen printed electrodes, and more recently, Ibupoto et al. [22] proposed a potentiometric sensor with ZnO nanotubes, with LOD of 5×10^{-4}, and 10^{-3} μg/mL, respectively.

This work reports the development of carbon nanotubes field effect transistor (NTFET) devices (with a back-gate and interdigitated configuration, and based on random networks of SWCNTs) as immunosensors for the label-free detection of CRP. The small sample volume, the low-cost, the easy analysis associated to the disposable devices, as well as the LOD lower than that of conventional assays for CRP detection will be highlighted as advantages for such NTFET immunosensors, which can be constitute a basis for the development of point-of-care testing methodologies for patients with high risk of cardiovascular diseases.

2. Material and methods

2.1. Reagents

Single-walled carbon nanotubes (SWCNTs), synthesized through cobalt–molybdenum catalysis (CoMoCAT, Southwest Nanotechnologies), sodium cholate (SC), C-reactive protein from human plasma (CRP), anti-human CRP antibodies (anti-CRP, produced in goat), Dulbecco's phosphate buffered saline (PBS, pH 7.4), bovine serum albumin (BSA), and Tween 20 were purchased from Sigma-Aldrich Química (Sintra, Portugal). PBS was used for the preparation of CRP stock solution (100 μg/mL), and corresponding serial dilutions between 10^{-4} and 10^{1} μg/mL, as well as for the anti-CRP stock solution (1 g/L), BSA (10 μg/mL), and Tween 20 (0.5%).

2.2. Preparation and characterization of SWCNT dispersion

SWCNTs were dispersed in distilled water with SC as an anionic surfactant, through the addition of 14 mL of aqueous solution of SC (0.2% w/v) to 4 mg of SWCNT. The experimental conditions for the dispersion of SWCNTs were previously optimized through the application of an experimental design, as reported elsewhere [23]. That is, the as-prepared SWCNT solution was processed for 60 min of sonication (on a water bath ultrasonicator, Ultrasonik 57H Ney, 400 W, 50/60 Hz) and then, for 5 min of centrifugation at a relative centrifugal force of $2000 \times g$ and 20 °C (centrifuge Medifriger BL-S of JP Selecta, Spain). Approximately a 70% fraction of the supernatant was collected for subsequent characterization and further use for the assembly of carbon nanotube field effect transistor devices, which were applied in this study as the disposable immunosensors for the CRP detection.

Raman spectroscopy was performed for the characterization of the dispersion of SWCNT in order to identify their electronic and vibrational structures as typical spectroscopic signature. Thus, Raman spectra (90–1900 cm^{-1}) were obtained with a Bruker RFS/100S Raman-FT spectrophotometer (Nd:YAG laser of 1064 nm, 100 mW power, spectral resolution of 4 cm^{-1}, and 1500 scans).

2.3. Device fabrication

The fabrication of disposable field effect transistor (FET) devices was performed at 3 inch wafer scale with silicon wafer as substrate (Sigma-Aldrich Química, Sintra, Portugal). The silicon wafer was passivated with silicon dioxide (SiO_2, 400 nm-thick layer) by plasma enhanced chemical vapor deposition (with Electrotech Delta CVD System). Thin layers of titanium (Ti, 10 nm-thick) and gold (Au, 100 nm-thick) were deposited on Si/SiO_2 substrate through physical vapor deposition by sputtering with Alcatel Magnetron Sputtering System. Optical lithography process (with Direct Write Laser 2.0, DWL, Heidelberg Instrument) was used to define the source (S) and drain (D) metal contacts, using a 1.5 μm-thick photoresist layer (PFR 7790G-27cP, JSR Corporation) coated in a standard spin coating system. Upon development, this patterned layer defines the mask for the ion beam etching (Nordiko 3000 Series) of the gold film. The photoresist film was then removed through immersion of the wafer in a stripper solution (Microstrip® 2001, Fujifilm) at 65 °C.

The silicon substrate was used as the back gate electrode; for that, a photoresist film (1.5 μm) was coated on the wafer, and the second mask (non-inverted) was defined by optical lithography with DWL system, and only an opening is defined in the resist. Then, 500 nm of SiO_2 were removed by reactive ion etching (with LAM Rainbow 440 System), and Cr/Au (50 nm-thick/100 nm-thick) films were deposited by ion beam deposition (Nordiko 3000 Series) immediately after ion beam etching (without vacuum break). The photoresist and the Cr/Au films were removed by liftoff, immersing the wafers in a Microstrip solution (Microstrip® 2001, Fujifilm) at 65 °C. The wafers were then cleaned with isopropanol and distilled water, and finally dried with a stream of nitrogen gas in a wet bench.

In order to promote individualized FET ($\sim 3 \times 2$ mm^2), the silicon wafer was diced using a dicing saw system (DISCO DAD 321), and each FET was then mounted into a printed circuit board (PCB), fixed and wirebonded with Al wires (25 μm Ø). Such wirebondings were

protected with a silicone gel (Elastosil E41, Wacker) making allowance for an open chamber (~1 mm Ø) for further sensing experiments, as shown in the lower inset of Fig. 2. The resulting individual FET devices have back-gate geometry and an interdigitated architecture configuration which allows a large surface area for sensing; each defined electrode has a 1.5 μm width, and a 1000 μm length.

FET surface was washed with acetone, 1-propanol, and distilled water, and then dried with a stream of nitrogen gas. Then, 1.2 μL of as-prepared SWCNT solution was deposited on a clean FET surface, and after a delay of 5 min, the droplet was blown off with a stream of nitrogen gas to form an SWCNT network bridging the FET electrodes. This same approach based on placing the SWCNT from liquid suspensions onto fabricated substrates has been already used after the definition of metallic electrodes [24]; however, several groups use the deposition of SWCNT before the definition of metal contacts through physical techniques such as drop casting or annealing [25,26].

The electrical characterization of the disposable carbon nanotube field effect transistor (NTFET) devices was performed at room temperature, in air, and in real-time, using a parameter analyzer (HP4155C, Japan), which was linked to a closed test fixture (Agilent 16442A, Japan) where the devices were positioned; in the test fixture, the drain, gate, and source of each FET were connected to respective terminals to provide electrical circuit for sensing measurements. In order to obtain an estimate of the instrumental variability, all measurements were carried out three times, and the reproducibility was evaluated performing all measurements in three individual FET devices. Before every experiment, the FET surface was washed with acetone and 1-propanol to remove any traces of grease, and twice with distilled water; then it was dried under a flow of nitrogen.

The geometry characteristics of fabricated FET devices were previously studied for enhancing device performance [27]: FET devices with 100 nm-thick of gold, a distance between the electrodes of 2.5 μm, and 10 electrodes (i.e., 5 source and 5 drain electrodes) were found to be the most suitable for further sensing experiments, due to their recorded lower resistances.

2.4. Immobilization of anti-CRP, detection of CRP, and control experiments

Due to the affinity of SWCNT with amino groups of antibodies, the immobilization of anti-CRP on surface of SWCNT was directly processed through a non-covalent adsorption [28]; unlike the covalent method, this process preserves the primary structures of SWCNT and consequently their electronic properties. A droplet of the anti-CRP solution (1 μL, 1 g/L) was pippeted on NTFET surface, which were stored overnight at 4 °C. In order to prevent evaporation of anti-CRP solution, each NTFET device was placed in a small Petri dish (10 cm Ø) hermetically sealed with parafilm. To remove unbound molecules, NTFET devices were then washed with PBS and dried with nitrogen for further electrical characterization. Two control assays were performed in parallel experiments in order to study the nonspecific binding of other compounds and possible interferences on SWCNT, as well as to study the specificity of fabricated NTFET devices to CRP analyte; the detailed experimental is reported in Appendix A (Supplementary materials).

For the detection of CRP, 1 μL of CRP solution at different concentrations (from 10^{-4} to 10^{2} μg/mL) were successively introduced into the silicone chamber of three individual NTFET devices, and incubated 15 min at room temperature. NTFET were washed with distilled water, dried with nitrogen, and their electrical characterization was immediately processed. The electrical measurements under dry conditions were employed in order to eliminate the influence of ions present in aqueous solutions, since FET devices are easily affected by ionic strength [17,19], and signal enhancement can be obtained when comparing with measurements in solutions systems [29]. The drain current (I_D) was measured as a function of drain voltage (V_D, between 0 and +2 V) to find the output characteristics of NTFET devices, after SWCNT deposition, antibody immobilization, and introduction of each CRP solution at various concentrations. The experiments in each condition were repeated three times. The transfer characteristics of such NTFET devices were also found with the measurement of I_D values against back-gate voltage (V_G, between −5 and +5 V) at a fixed drain voltage (V_D = +1 V). The changes in I_D values in each NTFET device after the exposure of any solution on the CNT surface are due to the variation of the flow of electrons through the nanotubes between the source and drain of each NTFET device.

As the detection of CRP antigen (I_{CRP}) depends on the interaction with its specific antibodies (anti-CRP) and in turn, with the extent of binding of anti-CRP onto SWCNT ($I_{anti\text{-}CRP}$), the analytical response (current change, ΔI_{CRP}) for the sensing experiments with the fabricated NTFET devices was considered as the change in I_D values for each CRP concentration after their interaction with antibody ($I_{CRP} - I_{anti\text{-}CRP}$). The analytical response from various NTFET devices was then plotted against the CRP concentration (between 10^{-4} and 10^{2} μg/mL) to obtain the calibration curve.

3. Results and discussion

3.1. Characterization of dispersion of single-walled carbon nanotubes and carbon nanotubes field effect transistors

Raman spectroscopy was used for the characterization of the dispersed SWCNT, which will further be used as conducting channel of carbon nanotubes field effect transistors (NTFET) devices. Fig. 1 shows the baseline corrected Raman spectrum obtained from the SWCNT dispersed in sodium cholate and used in this work.

From Fig. 1, the two active Raman modes of SWCNTs are present as first-order features; the low frequency radial breathing mode (RBM) is displayed between 100 and 300 cm^{-1}, and the high frequency G-bands are shown between 1550 and 1605 cm^{-1}.

The frequency of the RBM mode (ω_{RBM}), which is the feature of primary interest for SWCNT, allowed the determination of the average diameter of the SWCNT (d) as 1.8 nm, since a relation has been established [30]: $\omega_{RBM} = (234\ cm^{-1}\ nm/d) + 10\ cm^{-1}$. In turn, the G-bands have two main components (G^+ and G^-) which are not affected by the defects on SWCNT structure, and they are composed of several tangential modes due to stretching vibrations of the SWCNT sidewall C–C bonds [31]; the G^+ feature is observed at 1590 cm^{-1} due to in-plane vibrations along the nanotube axis, while the G^- feature at 1570 cm^{-1} is attributed to in-plane vibrations along the circumferential direction. On the other hand, the line shape of the G-band can be used to differentiate metallic and semiconducting SWCNTs; the pattern shown in Fig. 1 can be compared to that present in the work of Dresselhaus et al. [30] where the peak at 1590 cm^{-1} is associated with a semiconducting SWCNT. In turn, the weak frequency peak at ~1570 cm^{-1} (G^- band), with its commonly called Breit–Wigner–Fano line shape, is originated from the electron–phonon interactions in the metallic SWCNT.

An additional feature at about 1300 cm^{-1} (D-band) is attributed to a second-order Raman scattering process, which characterizes the structural disorder of the sp^2-hybridized carbon. In Fig. 1, such a band is very small which means that the impurities (e.g., carbonaceous materials), defects, and disorder

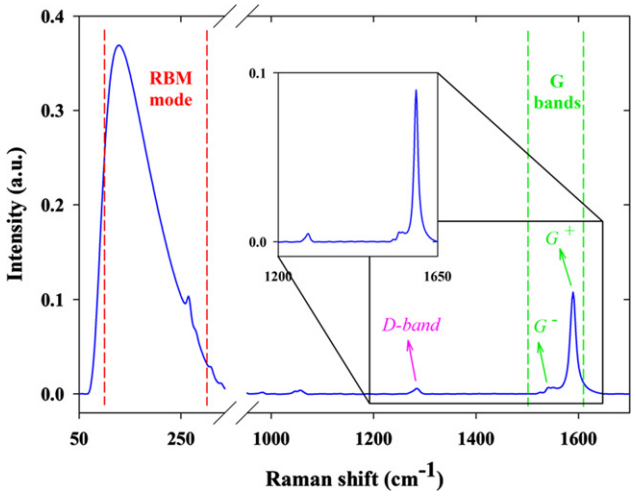

Fig. 1. Baseline corrected Raman spectrum of SWCNT dispersed in sodium cholate (recorded with 1064 nm laser excitation wavelength).

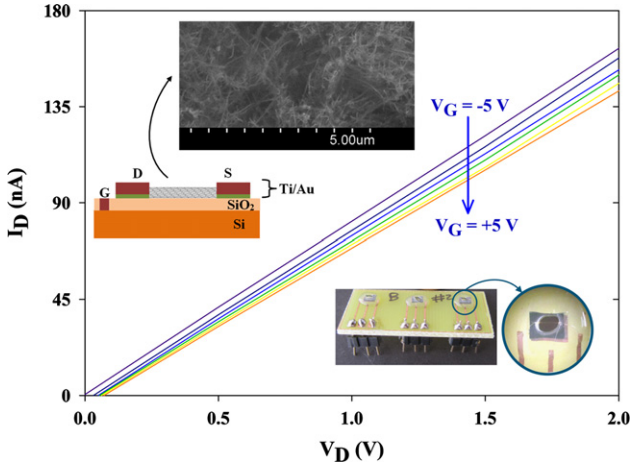

Fig. 2. Output characteristics (for V_G curves between −5 and +5 V) for one typical NTFET device. The lower inset shows photographic images of a PCB with three mounted FET and a zoom image of the silicone chamber where the sensing experiments were performed. The upper inset shows a schematic cross section of the NTFET device with a zoom SEM image (obtained from a SU-70 SEM microscope) of the network of SWCNT.

effects are minimal. On the other hand, the very low value of D/G^+ intensity ratio (~0.02) is an indicator of the quality of the dispersed SWCNT [30].

With the study of Raman spectrum, the electrical nature of the SWCNT network used for the assembly of NTFET devices can be identified. Thus, after the deposition of SWCNT onto a cleaned FET surface, the electrical properties of NTFET devices could be measured at room temperature and in real-time. All measurements were carried out on a closed box (test fixture), and the analysis of any solution was performed in the silicone chamber, as shown in the lower inset on the right of Fig. 2.

The output characteristics (I_D–V_D graph) of NTFET devices were checked, as shown in Fig. 2, for one typical NTFET device; various V_G curves (between −5 and +5 V) were plotted as the means of three successive measurements.

Fig. 2 shows that with increasing values of V_G (from −5 to +5 V), the I_D values decreased from 86.3 to 49.1 nA at $V_D = +1$ V, thus suggesting that the conduction process corresponds to hole transport as usually observed in SWCNT [32]. On the other hand, Fig. 2 and its upper inset also show that the ON/OFF ratio was as low as reported on other works with network-based devices [17–19], since the electrical signal is due to both semiconducting and metallic CNT. In addition, a SEM image was shown in the lower inset of Fig. 2, where a dense network of SWCNT was observed.

3.2. Immobilization of antibodies

Fig. 3 shows the output characteristics of a typical NTFET device (at $V_G = +1$ V) before and after the modification of NTFET surface with specific antibodies for CRP (anti-CRP).

The direct charge transfer is one of the proposed mechanisms about how the immobilization of charged analytes can affect the conductance of SWCNT [28]. Thus, and according to our experimental data shown in Fig. 3, the adsorption of a charged biomolecule at the nanotubes surface leads to a decrease of I_D values of 88% (at $V_D = +1$ V), which means that the immobilization of anti-CRP onto SWCNT has occurred. As reported in the work of Teker et al. [32], where a decrease in current of NTFET with the exposure of antibody molecules on the CNT channel occurred, the amine groups of antibodies provide electrons for nanotubes, reducing the number of holes (major charge carriers), and consequently also reducing the drain current.

3.3. Detection of CRP through NTFET devices

After the characterization of the NTFET devices (Figs. 2 and 3) and performing the control experiments (available in Appendix A, Supplementary materials), NTFET devices were tested for their sensing toward CRP. The detection of CRP of different concentrations (from 10^{-4} to 10^{2} μg/mL) was carried out through the measurement of drain current (at $V_G = +1$ V and $V_D = +1$ V) on three individual NTFET devices for each CRP concentration. The plot of the analytical response (current change, ΔI_{CRP}) is shown in Fig. 4; each data point represents an average value based on three successive measurements, which standard deviation is reflected in each error bar. The analytical response (ΔI_{CRP}) was considered as the change in drain current of NTFET devices by the interaction of CRP with their specific antibody ($\Delta I_{CRP} = I_{CRP} - I_{anti\text{-}CRP}$).

As a result of the binding events, i.e., antibody–antigen interactions, the geometrical deformation of nanotubes could occur, thus increasing the scattering centers among them [33], and specifically decreasing the current. This mechanism leads to differences in current behavior on NTFET devices. As shown in Fig. 4, the current change decreases with the increase of CRP

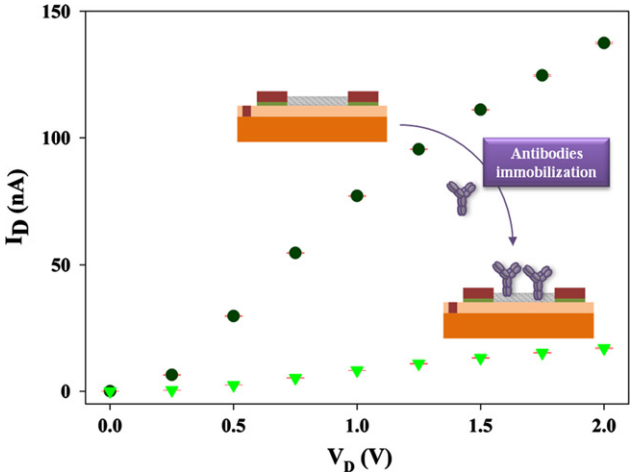

Fig. 3. Change in output characteristics (at $V_G = +1$ V) of a typical NTFET devices before (●) and after (▼) the incubation of anti-CRP (1 g/L) for 1 h; the errors bars represent the standard deviation of three successive measurements.

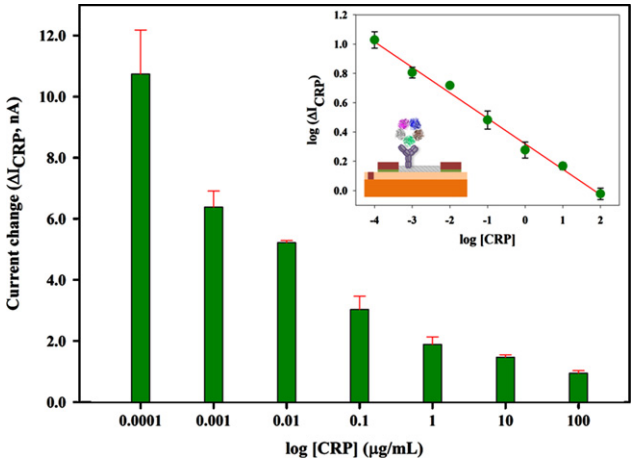

Fig. 4. Variation of the analytical response obtained from three individual NTFET devices per CRP concentration between 10^{-4} and 10^{-2} μg/mL (error bars represent the standard deviation). The inset graph shows the log–log regression analysis for the mean current change (response) of NTFET devices to CRP through immunoreaction (with schematic in inset graph).

concentrations from 10^{-4} to 10^{2} μg/mL. Such analytical response due to the lower variation of current change occurred in NTFET devices with the addition of increasing concentrations of CRP, could also be explained by the charge tunneling with the receptor analyte (anti-CRP), which reduces the mobility of holes (major carriers) [34] thus leading to the decrease of the current of devices.

The variability of the current change was estimated from the coefficients of variation (CV), which were calculated from the standard deviation observed in Fig. 4 for each CRP concentration. The current change for the three individual NTFET devices was 13.8, 8.2, 1.4, 14.5, 12.9, 5.6, and 8.8% for the successive decimal concentrations of CRP between 10^{-4} and 10^{2} μg/mL, respectively, with an average CV of 9.2 ± 4.7%. Thus, some variability on the response was recorded which can affect the reproducibility of devices. Such device-to-device variation after the interaction of biomolecules can be due to: (a) the random nature of nanotubes networks in terms of their chirality and their diameter; (b) variations in nanotubes density; (c) bundling of SWCNT networks; and (d) ratio of metallic and semiconducting nanotubes [35]. Such physical features can affect the electronic structure of SWCNT and consequently their mobility and current on each device. However, the ANOVA applied to the experimental data showed that there is not a statistically significant difference ($p=0.9582$) between various NTFET devices for the same concentration of CRP; as expected, it was also verified that there is a statistically significant difference ($p=1.3\times10^{-10}$) between the different levels of concentrations.

Based on the response of NTFET devices to CRP, as shown in Fig. 4, the best calibration model was sought for fitting the experimental data. In a first step, a logistic regression model based on a four-parameter logistic (4PL) curve, as shown in Fig. B.1 (available in Appendix B, Supplementary materials), was applied to the experimental data, since such calibration curve is recommended for limited reagent immunoassay [36], also being the most used calibration model of immunoassays [37]. An appropriate adjustment to the experimental data was obtained since acceptable value for the determination coefficients (R^2 of 0.9809; $p<0.0001$) was found as estimate of the goodness of fit; an adequate fit standard error of 0.316 was also found as measure of the regression variability. However, such 4PL model has the limitation of only the linear region of the function (with four calibration points from 10^{-1} to 10^{2} μg/mL) can be used for further determination of unknown concentrations, restricting the working range. In addition, the estimation of the concentrations of CRP from the 4PL model (through recovery functions) is inadequate since high recoveries of 155% and 36% were observed for the low and high plateaus of concentrations, respectively (with recoveries of 106 ± 25% for concentrations in the central region of 4PL curve); therefore, if the estimated concentrations are outside such linear range, the experiments should be repeated by diluting the sample. Then, in order to attempt to use the entire range of concentrations, the analytical response from Fig. 4 was plotted in a logarithmic scale as a function of the logarithmic concentration of CRP, as observed in the inset of Fig. 4. Then, a seven-point log–log curve fitting was obtained with better goodness of fitting ($r=0.996$, $p<0.001$ with adjusted r^2 of 0.991) than that obtained by 4PL model, with the poss ibility to use the broad range of CRP concentrations (seven orders of magnitude). A regression represented by $\log y=0.320(\pm 0.0152)-0.174(\pm 0.00680)\log x$ was obtained in a dynamic linear range from 10^{-4} to 10^{2} μg/mL (with fit standard error of 0.036), where y is the current change, and x is the concentration of CRP. Furthermore, the practical value of such disposable biosensing devices is here highlighted since it includes the normal concentration range of CRP levels in human blood serum (1–3 μg/mL), as well as it includes values below 1 μg/mL, and above 3 μg/mL of CRP. In other words, residual CRP levels between 0 and 0.1 μg/ml can be detected corresponding to the typical values for a healthy subject without any sign of inflammations, as well as it becomes possible to identify pathological cases (levels higher than 5 μg/mL). The developed NTFET devices also have the advantage of detecting CRP concentrations up to 100 μg/mL, which means that the high risk of cardiovascular diseases can be assessed when devices will be applied to real samples of blood serum. In addition, the dynamic linear range obtained with our devices ($10^{-4}-10^{2}$ μg/mL) is broadest than that of traditional high-sensitivity immunoassays for CRP in serum, which is between 5 and 10 μg/mL [4,5].

Concerning the sensitivity of NTFET devices, estimated as the experimental slope of the calibration curve (inset of Fig. 4), it is shown that a decrease of response (current change) by about 0.2% is observed for every 1% of CRP concentration increase. In turn, the limit of detection (LOD) obtained was about 10^{-4} μg/mL, considering the LOD as the detectable minimum concentration, which is better than the traditional immunochemical assays (LOD from 0.03 to 0.2 μg/mL) on 2–3 orders of magnitude. On the other hand, the LOD of the NTFET devices is much lower than the clinical relevant range of concentrations in serum, and it is better than other measurement systems used for the detection of CRP, for example, optical RNA-based aptasensor [8], chemiluminescence-based microfluidic system [9], and magnetic sensor [7], with LOD values of 5×10^{-3}, 1.25×10^{-2}, and 2.5×10^{-2} μg/mL, respectively. Furthermore, only 1 μL of CRP solution are used to the measurements in the range of 10^{-4} and 10^{2} μg/mL, being competitive with the above mentioned biosensing systems. Furthermore, Table C.1 (available in Appendix C, Supplementary materials) shows a favorable comparison of the analytical figures of merit (linear range and LOD) of this work against some recent biosensors for CRP detection.

According to International Union of Pure and Applied Chemistry [38], recovery testing (%) was performed through the comparison of the CRP concentration estimated by the regression model (inset of Fig. 4) with respective known concentration; average recoveries between 88% and 115% were obtained from the broad range of CRP concentrations.

In addition, it should be noticed that the disposable NTFET devices could become a potential alternative for the detection of CRP in saliva as a non-invasive sampling methodology, since the

linear range that should be covered in saliva is between 10^{-3} and 3×10^{-2} μg/mL [39] which is well within the range covered by our biosensing devices ($10^{-4}-10^{2}$ μg/mL).

4. Conclusions

The importance of the CRP as a significant and relevant proxy for assessing the risk of cardiovascular diseases, and other diseases associated to inflammatory processes, has been recognized from many years. Although some literature on NTFET biosensing has been conducted with semiconducting nanotubes, we demonstrate for the first time the possibility of detecting CRP by immunoreaction and electrical mechanism with nanotubes networks. The antibodies used for the specific interaction with CRP allow the detection of such inflammatory biomarker on a dynamic linear range over seven orders of magnitude (10^{-4} to 10^{2} μg/mL), from a log–log regression model ($r=0.996$; $p<0.001$). Thus, the NTFET devices are capable of detecting residual levels of CRP in healthy persons without any sign of inflammation, as well as critical levels of CRP responsible for pathological evidences. The cost-effectiveness of analysis as well as the rapid and simple use associated to the disposable NTFET devices makes them much more fit for purpose and advantageous than already available analytical systems. Furthermore, NTFET devices use a simple label-free methodology for sensing, and obtaining lower LOD than the conventional immunoassays, thus becoming an alternative as the basis for the use of point-of-care testing methodology for patients with high risk of cardiovascular diseases.

Acknowledgments

This work was funded by FEDER under the Operational Program for Competitiveness Factors (COMPETE), and by National funds via FCT (Fundação para a Ciência e a Tecnologia, Portugal) within the framework of the research project CARDIOSENSOR (references FCOMP-01-0124-FEDER-010902 and PTDC/SAU-BEB/099042/2008, respectively). This work was also funded through scholarships (references SFRH/BD/60429/2009, SFRH/BPD/65410/2009, and SFRH/BPD/73781/2010) under QREN-POPH funds, co-financed by the European Social Fund and Portuguese National Funds from MCTES. INESC-MN also acknowledges FCT funding through the Associated Lab—Instituto de Nanotecnologias (IN). The authors also acknowledge Maria Celeste Azevedo from the Department of Chemistry (University of Aveiro, Portugal) and Doctor Florinda Costa from the Department of Physics (University of Aveiro, Portugal) for the help on the laboratory facilities of Raman spectroscopy, and scanning electron microscopy, respectively.

Appendix A. Supplementary materials

Supplementary materials associated with this article can be found in the online version at http://dx.doi.org/10.1016/j.talanta.2013.03.007.

References

[1] R.R. Packard, P. Libby, Clin. Chem. (Washington, DC, U.S.) 54 (2008) 24–38.
[2] V.L. Roger, A.S. Go, D.M. Lloyd-Jones, E.J. Benjamin, J.D. Berry, W.B. Borden, D.M. Bravata, S. Dai, E.S. Ford, C.S. Fox, H.J. Fullerton, C. Gillespie, S.M. Hailpern, J.A. Heit, V.J. Howard, B.M. Kissela, S.J. Kittner, D.T. Lackland, J.H. Lichtman, L.D. Lisabeth, D.M. Makuc, G.M. Marcus, A. Marelli, D.B. Matchar, C.S. Moy, D. Mozaffarian, M.E. Mussolino, G. Nichol, N.P. Paynter, E.Z. Soliman, P.D. Sorlie, N. Sotoodehnia, T.N. Turan, S.S. Virani, N.D. Wong, D. Woo, M.B. Turner, Circulation 125 (2012) 2–220.
[3] B. Clyne, J.S. Olshaker, J. Emerg. Med. 17 (1999) 1019–1025.
[4] R. Dominici, P. Luraschi, C. Franzini, J. Clin. Lab. Anal. 18 (2004) 280–284.
[5] Food and Drug Administration, Guidance for industry—review criteria for assessment of C-reactive protein (CRP), high sensitivity C-reactive protein (hsCRP) and cardiac C-reactive protein (cCRP) assays, 2005. 〈http://www.fda.gov/downloads/MedicalDevices/DeviceRegulationandGuidance/GuidanceDocuments/UCM071017.pdf〉 (accessed 11.11.12).
[6] C.I.L. Justino, T.A. Rocha-Santos, A.C. Duarte, TrAC, Trends Anal. Chem. 10 (2010) 1172–1183.
[7] M.H.F. Meyer, M. Hartmann, H.J. Krause, G. Blankenstein, B. Mueller-Chorus, J. Oster, P. Miethe, M. Keusgen, Biosens. Bioelectron. 22 (2007) 973–979.
[8] A. Bini, S. Centi, S. Tombelli, M. Minunni, M. Mascini, Anal. Bioanal. Chem. 390 (2008) 1077–1086.
[9] Y.-N. Yang, H.-I. Lin, J.-H. Wang, S.-C. Shiesh, G.-B Lee, Biosens. Bioelectron. 24 (2009) 3091–3096.
[10] A. Quershi, Y. Gurbuz, W.P. Kang, J.L. Davidson, Biosens. Bioelectron. 25 (2009) 877–882.
[11] K. Balasubramanian, M. Burghard, Anal. Bioanal. Chem. 385 (2006) 452–468.
[12] C. Li, M. Curreli, H. Lin, B. Lei, F.N. Ishikawa, R. Datar, R.J. Cote, M.E. Thompson, C. Zhou, J. Am. Chem. Soc. 127 (2005) 12484–12485.
[13] K. Maehashi, K. Matsumoto, Y. Takamura, E. Tamiya, Electroanalysis 21 (2009) 1285–1290.
[14] J.P. Kim, B.Y. Lee, J. Lee, S. Hong, S.J. Sim, Biosens. Bioelectron. 24 (2009) 3372–3378.
[15] S. Okuda, S. Okamoto, Y. Ohno, K. Maehashi, K. Inoue, K. Matsumoto, J. Phys. Chem. C 116 (2012) 19490–19495.
[16] E.L. Gui, L.-J. Li, K. Zhang, Y. Xu, X. Dong, X Ho, P.S. Lee, J. Kasim, Z.X Shen, J.A. Rogers, S.G. Mhaisalkar, J. Am. Chem. Soc. 129 (2007) 14427–14432.
[17] C.C. Cid, J. Riu, A. Maroto, F.X. Rius, Curr. Nanosci. 4 (2008) 314–317.
[18] C.C. Cid, J. Riu, A. Maroto, F.X. Rius, Analyst 133 (2008) 1005–1008.
[19] R.A. Villamizar, A. Maroto, F.X. Rius, Anal. Bional. Chem. 399 (2011) 119–126.
[20] F.N. Ishikawa, M. Curreli, C.A. Olson, H.-I. Liao, R. Sun, R.W. Roberts, R.J. Cote, M.E. Thompson, C. Zhou, ACS Nano 4 (2010) 6914–6922.
[21] M. Buch, J. Rishpon, Electroanalysis 23 (2008) 2592–2594.
[22] Z.H. Ibupoto, N. Jamal, K. Khun, M. Willander, Sens. Actuators, B 166 (2012) 809–814.
[23] C.I.L. Justino, A.C. Freitas, T.A.P. Rocha-Santos, A.C. Duarte, Talanta 89 (2012) 105–108.
[24] A. Javey, Q. Wang, A. Ural, Y. Li, H. Dai, Nano Lett. 2 (2002) 929–932.
[25] S.J. Wind, J. Appenzeller, R. Martel, V. Derycke, P. Avouris, Appl. Phys. Lett. 80 (2002) 3817–3819.
[26] J.-A. Lim, N. Phiboolsirichit, S. Mubeen, Y. Rheem, M.A. Deshusses, A. Mulchandani, N.V. Myunga, Electroanalysis 22 (2010) 99–105.
[27] C.I.L. Justino, T.A.P. Rocha-Santos, J.P. Amaral, S. Cardoso, A.C. Duarte, Solid State Electron. 81 (2013) 32–34.
[28] G. Gruner, Anal, Bioanal. Chem. 384 (2006) 322–335.
[29] C.S. Ah, C.W. Park, J.-H. Yang, J.S. Lee, W.-J. Kim, H. Chung, I.B. Baek, J. Kim, G.Y. Sung, Biosens. Bioelectron. 33 (2012) 233–240.
[30] M.S. Dresselhaus, G. Dresselhaus, R. Saito, A. Jorio, Phys. Rep. 409 (2005) 47–99.
[31] M.E. Itkis, D.E. Perea, R. Jung, S. Niyogi, R.C. Haddon, J. Am. Chem. Soc. 127 (2005) 3439–3448.
[32] K. Teker, E. Wickstrom, B. Panchapakesan, IEEE Sensors J. 6 (2006) 1422–1428.
[33] A. Kojima, C.K. Huon, T. Kamimura, M. Maeda, K. Matsumoto, Jpn. J. Appl. Phys. 44 (2005) 1596–1598.
[34] R.A. Villamizar, A. Maroto, F.X. Rius, I. Inza, M.J. Figueras, Biosens. Bioelectron. 24 (2008) 279–283.
[35] J.N. Tey, P.M. Wijaya, Z. Wang, W.H. Goh, A. Palaniappan, S.G. Mhaisalkar, I. Rodriguez, S. Dunham, J.A. Rogers, Appl. Phys. Lett. 94 (2009) 013107.
[36] J.A. Little, Chromatographia 59 (2004) 177–181.
[37] J.F. Robinson-Cox, J. Immunol. Methods 186 (1995) 79–88.
[38] K. Danzer, M. Otto, L.A. Currie, Pure Appl. Chem. 76 (2004) 1215–1225.
[39] Testing protocol, Cat. # 1-3302, Salimetrics™. 〈http://www.salimetrics.com/salivary-assay-kits〉 (accessed 21.02.13).